https://doi.org/10.22226/2410-3535-2023-1-20-27

Carbon matrix nanostructured composites as a new type of supercapacitor electrode materials

Yu. A. Zakharov†,[1], G. Yu. Simenyuk[1], T. O. Sergina[1], N. V. Ivanova[2], T. A. Larichev[1,2], I. Yu. Zykov[1], Yu. N. Dudnikova[1]

†zakharovya@iccms.sbras.ru

[1]Federal Research Centre of Coal and Coal Chemistry, SB RAS, Kemerovo, 650000, Russia
[2]Kemerovo State University, Kemerovo, 650000, Russia

Carbon matrix nanocomposites C/Au and C/Mn_xO_y are obtained by a reduction of $HAuCl_4$ and $KMnO_4$ precursor solutions with single-walled carbon nanotubes or highly porous carbon materials obtained by high-temperature alkaline activation of various metamorphism degree coals. The morphology of the nanocomposite materials is studied by the electron microscopy. It is found that the filler introduction slightly reduces the specific surface of matrices and, due to the blocking of meso- and micropore volumes, filler nanoparticles do not precipitate in the pores of a predominantly microporous matrix and partially decorate them in mixed-type matrices (meso- and micropores). Nanocomposites have been studied as supercapacitor electrode materials. It is established that decorating the matrix surface with both types fillers (Au, which increases the electrical double layer capacitance, and Mn_xO_y, which is electrochemically active in a given potential window due to the occurrence of Red-O_x electrode processes) results in an increase in the supercapacitor electrodes capacitance. The most significant effect is observed for composites based on the SWCNT and highly porous Boghead in the region of high potential scan rates by a factor of 3.4 – 4.5, and in the region of low rates (2.5 – 2.8), depending on the filler. The results obtained allow one to consider the composites C/Au and C/Mn_xO_y as promising materials for the development of SC electrodes.

Keywords: Carbon matrices, gold and manganese oxide nanoparticles, nanostructured composites, electrode materials, supercapacitors.

1. Introduction

Despite the large number of published works and significant progress in the development of electrode materials for supercapacitors (SCs) based on the allotropic carbon forms of various morphologies (single-walled carbon nanotubes (SWCNT), multi-walled carbon nanotubes (MWCNT), graphene-like structures, highly porous carbon materials (HPCM)), which have high electrical capacitance characteristics [1–7], the general problem of combining the required level of electrode functional characteristics with the "cost of one farad" remains unresolved. In this regard, and with the growing need for SCs for mass operation (electrical energy accumulation to ensure the temporal stability of power systems based on cyclically or aperiodically operating generating sources, electric vehicles, backup power systems, etc.), the relevance of works on the development of other variants of SC electrodes is increasing [8–10]. One of the main directions is the development of carbon-matrix nanocomposite electrode materials based on relatively inexpensive but highly functional C-matrices filled with nanoparticles (NPs) of electrochemically active compounds and/or facilitating active charge accumulation due to the electrical double layer (EDL) formation. In the first case, the total specific electrical capacitance of the material increases due to the pseudocapacitive component addition as a result of the occurrence of electrode Red-Ox reactions; in the second case, due to non-faradaic EDL effects at the electrode/electrolyte interface, which are more pronounced than at the carbon/electrolyte interface. At the same time, the most important task in determining the prospects for the "carbon-matrix nanocomposite approach" is the implementation of the maximum possible effects of increasing the capacitance and other functional characteristics of nanostructured composites (NSCs) formed on the basis of promising types of C-matrices filled with nanoparticles of various types.

In the present work, within the framework of solving the above problem, we consider, for the first time, two types of NSCs formed on the basis of C-matrices of different morphologies (SWCNT [11] and HPCM [12] synthesized from bituminous coals with different metamorphism degrees) and filled with NPs, which, as shown by us earlier [6,13–16], most efficiently accumulate the electric charge by alternative mechanisms of EDL formation (Au) and electrode Red-Ox reactions (Mn_xO_y). The increase in the electrical capacitance upon introduction of these types of fillers into matrices indicates both the general promise of the "carbon matrix nanocomposite approach" and the possibility of manufacturing supercapacitors based on the considered NSC electrode materials with high functional characteristics.

2. Materials and experimental methods

2.1. Reagents and materials

Three types of carbon materials were used as matrices: TUBALL SWCNT (OCSiAl, Novosibirsk), highly porous carbon materials Boghead and CAK (Carbonized anthracite with KOH activation), obtained under the conditions similar to [17] by alkaline activation (KOH/C = 2:1) at 800°C from coals with varying metamorphism degrees: Boghead (sapropelic coal type, low metamorphism degree, Taimylyrskoe deposit, Yakutia, Russia) and anthracite (the highest coalification degree, Kiyzassky section, Kuzbass, Russia), respectively. $HAuCl_4$ solutions are used as precursors in the Au/C nanocomposites synthesis, and $KMnO_4$ solutions were used as precursors in the synthesis of Mn_xO_y/C NSC. All reagents were of analytical grade.

2.2. Synthesis of nanostructured composites

The preparation of composites was carried out by means of the reduction of precursor solutions directly by the matrix itself, without additional reducing agents [6,18]. The carbon matrix was placed in bottles and impregnated with 10^{-4} M $KMnO_4$ or 10^{-4} M $HAuCl_4$ solutions. The impregnation was carried out in portions, in several stages (20 times) to implement the conditions for layer-by-layer filler deposition. Each subsequent solution portion was poured after the previous one had completely reacted. The control over the process completion was carried out spectrophotometrically, by the absence of MnO_4^- or $AuCl_4^-$ ions in the filtrate. In the case of Mn_xO_y, the reaction proceeded at 60°C for 20 – 60 min; therefore, the next portion was added after 20 – 60 min, depending on the matrix type. When creating Au/C composites, a new solution portion was poured every other day to ensure the completeness of the precipitation and reduce the loss of gold.

The technique is presented in detail in [6,13,18].

2.3. Characterization of composites

In this work, the main attention is paid to the study of the morphology, porous structure, and electrical capacitance characteristics of NSCs and C-matrices. Previously, some of these systems were characterized using the X-ray diffraction method, by which the phase composition and the coherent scattering region sizes of fillers in NSC were estimated, and thermally stimulated processes were studied by the derivative mass spectrometry [9,15,19]. Micrographs of the composites were obtained using a JEOL JEM 2100 transmission electron microscope (TEM) (Japan) and a JEOL JSM-6390 LV scanning electron microscope (SEM).

The porous structure parameters for C-matrices and NSCs were determined from the low-temperature (77 K) N_2 sorption isotherms recorded by an ASAP-2020 Micrometrics analyzer. Using the BET, BJH, DFT, etc. methods, the adsorption/desorption isotherms data were processed and the specific surface, pore volumes, including mesopores, average pore size, and pore size distributions (PSD) in the meso- and micropore regions were calculated. The technique is given in [12, 20 – 23].

Electrochemical properties of electrode materials from the initial carbon matrices and NSCs were investigated in a two-electrode electrochemical cell using PARSTAT 4000 potentiostat (Ametek, USA) and the VersaStudio software. A Nafion membrane was used as a separator, and a 30% KOH aqueous solution was used as an electrolyte; the mass of each electrode was equal to 0.01 g.

To prepare the electrode material, a few drops of a 30% KOH solution were added to a 10 mg sample of the NSC, the resulting mixture was ground in an agate mortar to a homogeneous state, and applied to graphite rods ∅6 mm used as current collectors. The design of the cell made it possible to provide a constant mechanical force of the electrode material prepressing by the current collectors in a series of measurements.

To measure the capacitance characteristics of the C-matrices, a symmetrical electrochemical cell, where both electrodes were matrices, was used. Electrochemical studies of NSC electrodes were carried out in an asymmetric cell, where NSC was used as the working electrode material, and the corresponding matrix as the counter electrode.

Cyclic voltametric (CV) experiments were carried out in the potential window (−1.0 ÷ +1.0) V, the potential sweep rate was varied from 2.5 to 300 mV/s. A wide scanning rate range made it possible to consider the difference in the behavior of the systems. The electrical capacitance of a whole cell C_{cell} was calculated by the formula

$$C_{cell} = \frac{q}{\Delta U \times m}, \quad (1)$$

where q is the electric charge accumulated by the cell, C; ΔU is the potential difference, V; m is the electrode material mass, g.

The working electrode capacitance ($C_{w.e.}$ or C) was estimated by the formula

$$C_{w.e.} = \frac{C_{cell} \times C_{c.e.}}{C_{c.e.} - C_{cell}}, \quad (2)$$

where C_{cell} is the cell capacitance and $C_{c.e.}$ the counter electrode capacitance.

3. Results and Discussion

3.1. SWCNT based composites

TEM micrographs of SWCNTs confirm the well-known high degree of their coalescence by outer walls with the formation of dense "ropes" of 10 – 100 nm in diameter composed of individual tubes (Fig. 1a, b). The diameter of individual tubes corresponds to that specified in the certificate (1 – 2 nm); extended channels between coalesced SWCNTs have a complex morphology: different widths, closed (isolated) sections are observed due to the aperiodic tubes closure.

The sizes of individual Au and Mn_xO_y NPs are noticeably larger than the diameters of the tube channels and the spaces between the coalesced SWCNTs; this implies that the filler NPs are deposited on the outer surface of the "ropes". In the SWCNT/Au NSC, they decorate the ropes surface (Fig. 1c),

Mn_xO_y nanoparticles form "islands". The proportion of the SWCNT matrix surface covered with fillers is 10 – 20%.

Previous X-ray diffraction experiments showed [24] that the Au particles introduced into SWCNTs were formed with an fcc structure in the form of two size fractions: particles with sizes 9 –12 nm, which coincide with the TEM data (estimated from the reflection broadening according to the Scherrer equation), and aggregates with sizes in the range of tens of nanometers. Aggregates of SWCNT Mn_xO_y deposited on the matrix are composed of almost X-ray amorphous nanoparticles; XRD diffraction reflections are very broad and weakly expressed, which does not allow determining the phase composition of the filler.

The typical N_2 adsorption-desorption isotherms on the SWCNT (matrix), NSC SWCNT/4% Au and NSC SWCNT/2%Mn_xO_y are shown in Fig. 2 a; they belong to the IV type according to the IUPAC classification. The observed capillary-condensation hysteresis loops correspond to the H3 type, which indicates the slit-like pore presence in the samples, which, according to Fig. 1a, b, can be attributed to SWCNT channels, and (or) to the pores between the coalesced SWCNT walls. Their sizes on the distribution curves (Fig. 2 b) correspond to the TEM results.

The nature of mesopores with a wide size distribution (20 – 60 nm) can be associated with the pore space in the aggregates and places of "ropes" interweaving; from the practical similarity of the corresponding extrema on the pore distribution curves for SWCNT, NSC SWCNT/Au and SWCNT/Mn_xO_y, it follows that they refer to the matrix and the pore distributions are practically independent of the filler types and their content. The matrix and NSC textural characteristics are summarized in Table 1.

In accordance with the sorptometry results and data on the NSCs morphology, filler nanoparticles do not form on the meso- and micropores surface, practically do not affect their parameters and, being deposited on the outer "ropes" surface, only weakly block the pores and slightly reduce the S_{BET}.

CV curves for electrochemical cells with SWCNT electrodes, asymmetric cells SWCNT/2% Au and SWCNT/4% Mn_xO_y are presented in Fig. 3 a, b, c. In Fig. 3 d, the dependence of the specific electrical capacitance of the electrodes on the potential scan rate is shown. The electric charge accumulation process upon SWCNTs and NSCs electrodes polarization proceeds nontrivially. The CV curves for symmetrical cells with SWCNT electrodes differ in their shape from the CVs for electrodes with charge accumulation in the EDL. The pseudocapacitive component contribution probably is due to the occurrence of electrode Red-Ox reactions involving surface functional groups and, possibly, an insignificant amount of iron NPs used as a catalyst in the SWCNT preparation. Accordingly, a noticeable increase in the specific capacitance is observed with a decrease in the scanning rate, due to the pseudocapacitive component contribution.

The SWCNT electrical capacitance values are not too large, as it can be predicted from their high specific surface area. It is

Table 1. Pore structure parameters of the SWCNT matrix and composites.

No.	Sample name	S_{BET}, m^2/g	V_Σ, cm^3/g	V_{micro}, cm^3/g	V_{meso}, cm^3/g	D_{pores}, Å
1	SWCNT	1077	1.426	0.303	1.043	53
2	SWCNT/2%Au	942	1.346	0.248	1.018	57
3	SWCNT/4%Au	912	1.265	0.239	0.946	55
4	SWCNT/2%Mn_xO_y	900	1.340	0.225	1.049	59

Notes: S_{BET} — specific surface area, m^2/g; V_Σ — total pore volume, cm^3/g; V_{micro}, V_{meso} are the micro- and mesopores volumes, cm^3/g, respectively; D_{pores} is the average pore diameter, Å. $\Delta V_\Sigma \simeq \Delta V_{micro} + \Delta V_{meso}$.

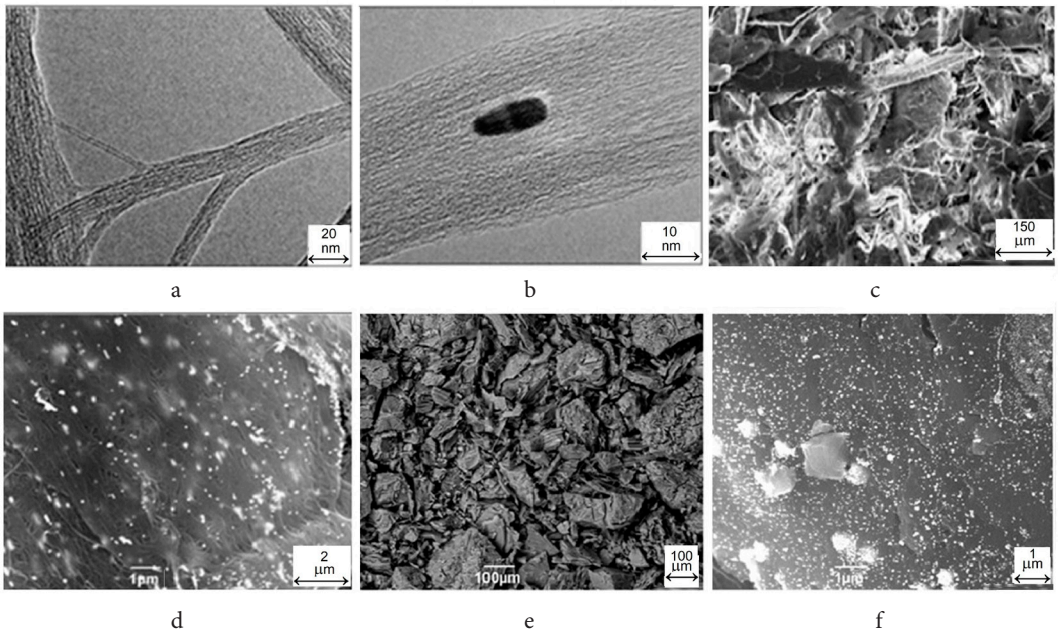

Fig. 1. TEM (a, b) and REM (c – f) images for SWCNT (a), SWCNT/4%Au (b, c), SWCNT/2%Au (d), CAK (e) and CAK/2%Au (f).

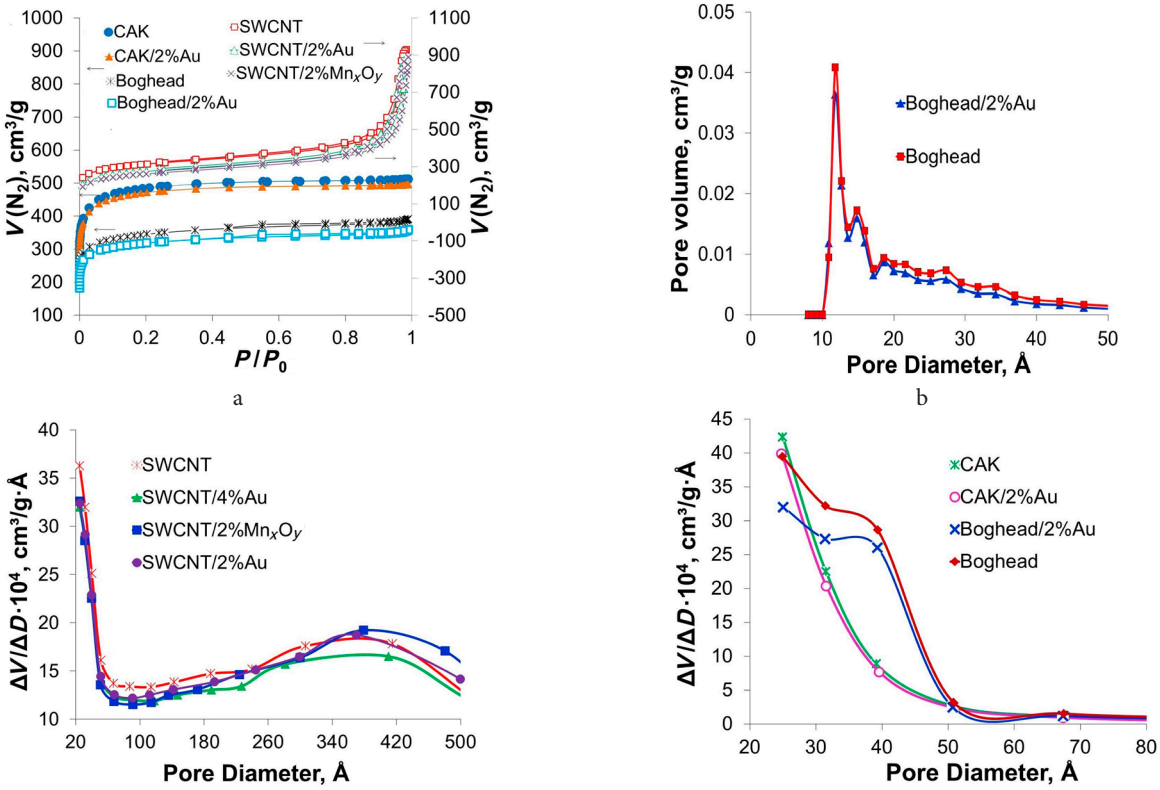

Fig. 2. (Color online) Typical adsorption isotherms (a), micropore distribution (calculated on DFT) (b), PSD calculated by BJH (c, d) for SWCNT (c) Boghead, CAK (d) and NSC on their basis.

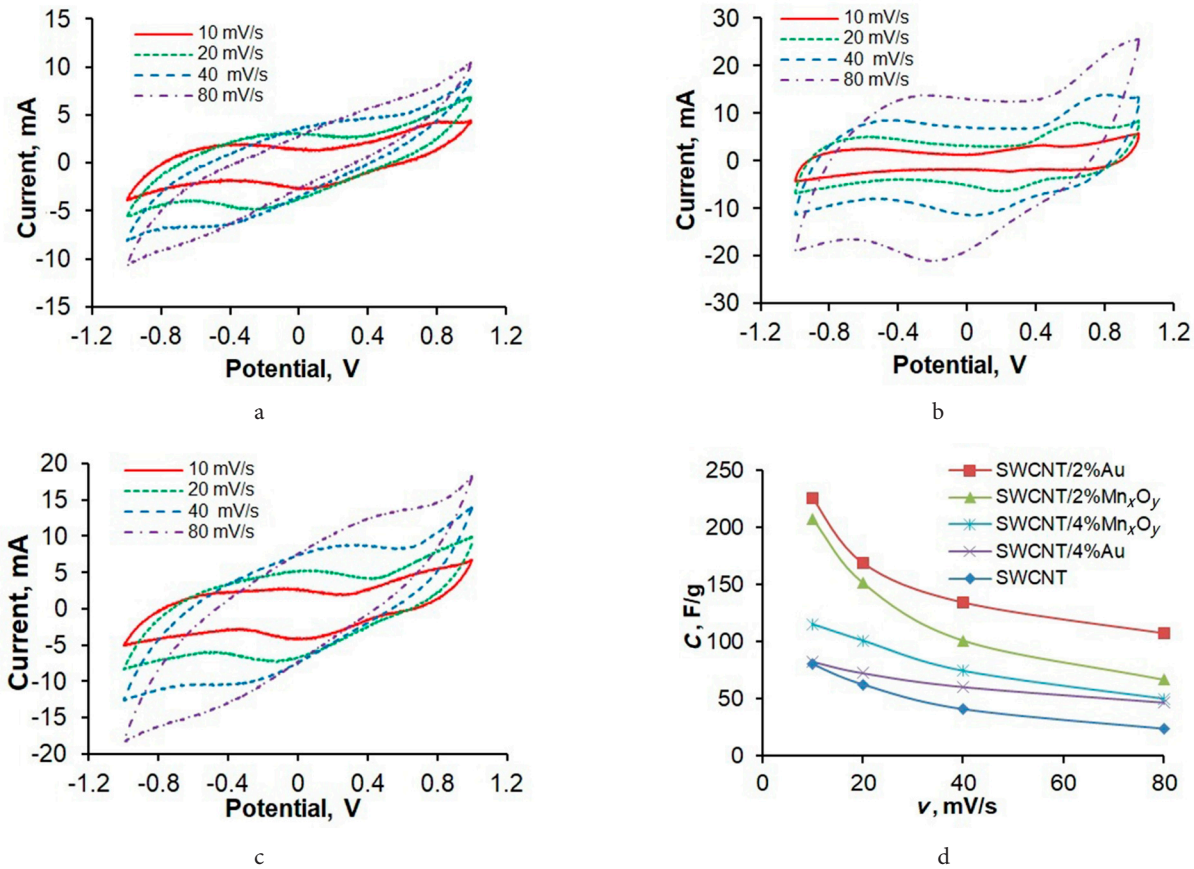

Fig. 3. (Color online) CV curves of a symmetric cell with electrodes based on the SWCNT matrix (a) and asymmetric cells with working electrodes based on NSC SWCNT/2%Au (b) and SWCNT/4% Mn_xO_y (c). Dependences of the specific electrical capacitance on the potential scan rate (d).

explained by some factors such as the small internal channels diameter of SWCNT (Fig. 1), their dense coalescence with outer walls, and the well-known C-tubes hydrophobicity. As a result, a lot of the SWCNT total surface, being available for the N_2 physical sorption (S_{BET} — Table 1), is difficult to access for the electrolyte. The deposition of Au layers on the outer SWCNT "ropes" surface results in a noticeable increase in capacitance, which is more pronounced in the high scanning rate region. The presence of Au layers brings the CV curves closer to the rectangular shape characteristic for the electric charge accumulation in EDL.

Our results are consistent with the data of other authors [25–27], the gold NPs increase the electrical conductivity of the composite by providing a tighter contact between nanotubes, which results in an increase in the EDL capacitance and a more pronounced manifestation of the pseudocapacitive component represented by anodic/cathodic peaks in the potential ranges (0.5 ÷ 0.8) V and (0.2 ÷ –0.4) V, respectively. Optimal Au concentration in Au/MWCNT in [26] was 5–10 wt.%, leading to enhanced specific capacitance value of 110–116 F/g in comparison with initial MWCNT (67 F/g); but a higher loading of the composite (20–40% Au NPs) expectedly reduces the capacitance (16 F/g at 40% of Au) due to the blocking of pores and the surface of the C-matrix. In our research, the optimal Au content equals 2 wt.%, which makes it possible to significantly reduce the consumption of precious metal in composites.

The addition of Mn_xO_y NPs into the SWCNT also leads to an increase in the electric capacitance; the pseudocapacitance contribution associated with the Red-Ox Mn compounds transformations is noticeable. The electrocapacitive properties of NSC on the basis of Mn_xO_y are widely variable depending on their preparation conditions [28–29]. It is of interest to optimize the conditions for NSC synthesis in order to achieve a record increase in the capacitance of the carbon materials. The capacitance of composite electrodes of optimal composition in our work is about 2.5–3 times greater than the capacitance of the original nanotubes. A similar behavior was also observed by us earlier in [19] for NSC C-matrix/Mn_xO_y based on MWCNTs.

3.2. HPCM based composites

SEM micrographs show the complex surface structure of HPCM obtained from coal raw materials. Au and Mn_xO_y NPs are deposited on the matrix surface in the form of relatively large aggregates (with sizes of tens of nanometers, Fig. 1d, f). It is difficult to determine the degree of meso- and macropores blocking by them, but, based on the estimated coverage degree of the total surface (no more than 10–15%), it should not be significant.

Typical adsorption-desorption isotherms for matrices (Boghead and CAK) and corresponding NSCs, as well as PSD curves, are shown in Fig. 2. The calculated textural characteristics of the samples are summarized in Table 2. The resulting isotherms are of type I according to the IUPAC classification (practically horizontal plateau); the samples are characterized by type H4 capillary-condensation hysteresis, indicating the presence of micropores.

An analysis of the obtained results shows that the CAK matrix obtained from anthracite with a high metamorphism degree, as expected, is predominantly microporous (the volume fraction of micropores is 90%), while the Boghead matrix obtained from coal with a low degree metamorphism has a relatively high (about 20 vol.%) fraction of mesopores (Fig. 2d). It should be noted that the size distribution of micropores is close for both matrices (Fig. 2b), there is an insignificant shift for CAK towards smaller sizes (Table 2).

The introduction of fillers into the CAK matrix practically does not change the volume and size distribution of mesopores (Fig. 2d) and slightly reduces the micropores volume (Table 2); more noticeable relative changes are observed for NSCs based on the Boghead matrix (Fig. 2d), while the average size of large micropores also slightly decreases (Table 2). In all cases, there is a balance in the decrease in the pore volume, which indicates the correctness of the determinations carried out by various calculation methods.

On a whole, according to the SEM results, aggregates of fillers formed on the surface of matrices weakly block pores, and in the case of Boghead based NSC, they are also deposited in insignificant amounts on the mesopores and micropores surface.

Typical CV curves of symmetrical electrochemical cells with HPCM electrodes and asymmetric cells with working electrodes from the NSCs under consideration are shown in Figs. 4 and 5.

The shape of the CV curves for the Boghead matrix and NSCs is close to a rectangular one, which is characteristic of charge accumulation in EDL. Weak manifestations of faradaic processes are noticeable only for NSC with Mn_xO_y at low scanning rates (Fig. 4c). For the CAK matrix and the corresponding NSCs, the shape of the curves is distorted, possibly due to diffusion limitations during the formation of EDL on the surface of a ramified CAK micropore system.

Comparing the results presented in Fig. 4d and 5d with the sorption data, it follows that at high scanning rates, the electric charge accumulates mainly in the mesopores of the HPCM, which are more developed in the Boghead matrix. As a result, this matrix is characterized by higher values of the specific electrical capacitance. Micropores with a typical size distribution shown in Fig. 2b are practically inaccessible to the electrolyte in the CAK HPCM and, probably, poorly accessible in Boghead, which follows from a comparison of the electrical capacitance characteristics of the matrices with the degree of development of micropores in them.

Table 2. Pore structure parameters of the HPCM matrix and composites.

No.	Sample name	S_{BET}, m²/g	V_{Σ}, cm³/g	V_{micro}, cm³/g	V_{meso}, cm³/g	D_{pores}, Å
1	Boghead	1302	0.600	0.397	0.106	19
2	Boghead / 2 % Au	1206	0.551	0.374	0.092	18
3	CAK	1836	0.792	0.604	0.066	17
4	CAK / 2% Au	1790	0.766	0.572	0.061	17

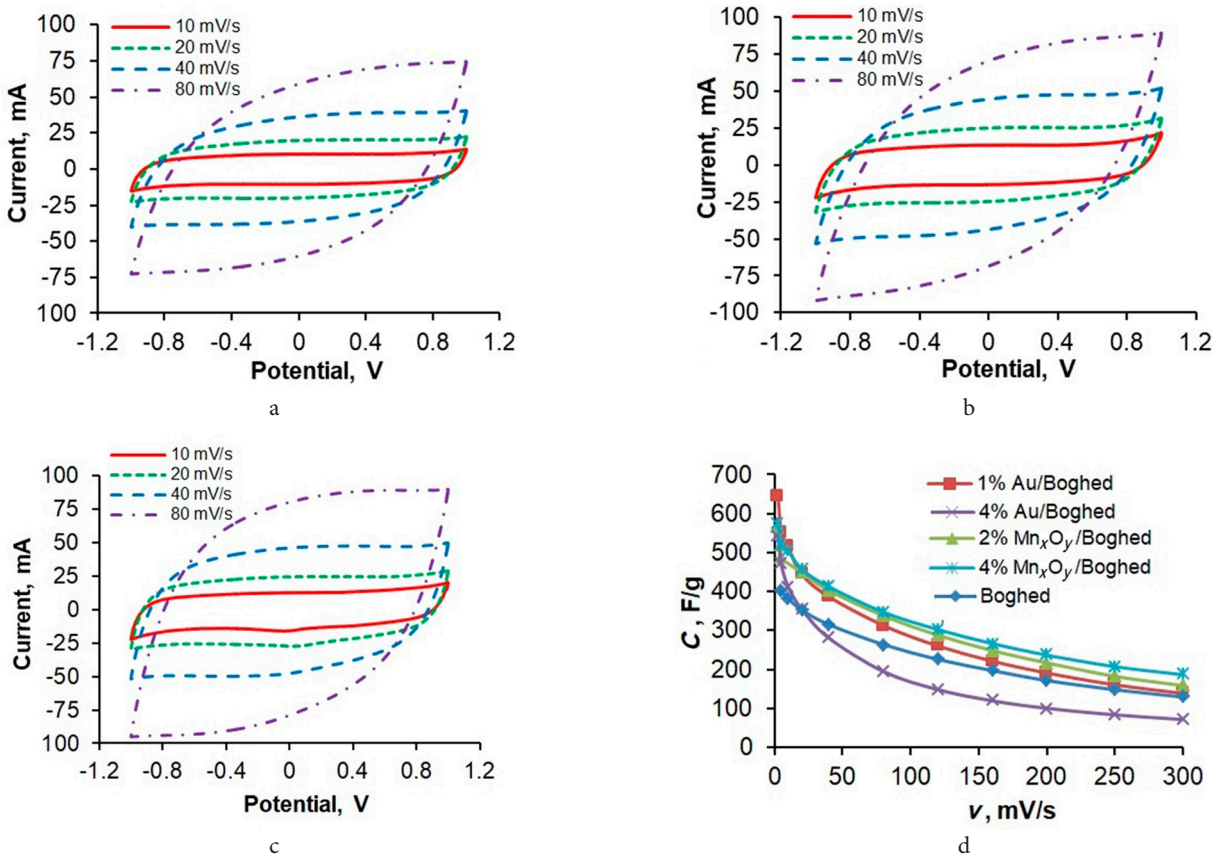

Fig. 4. (Color online) CV curves of a symmetrical cell with electrodes based on the Boghead matrix (a) and asymmetric cells with working electrodes based on NSC Boghead/1% Au (b) and Boghead/4% Mn_xO_y (c). Dependences of the electrode specific capacitance on the potential scan rate (d).

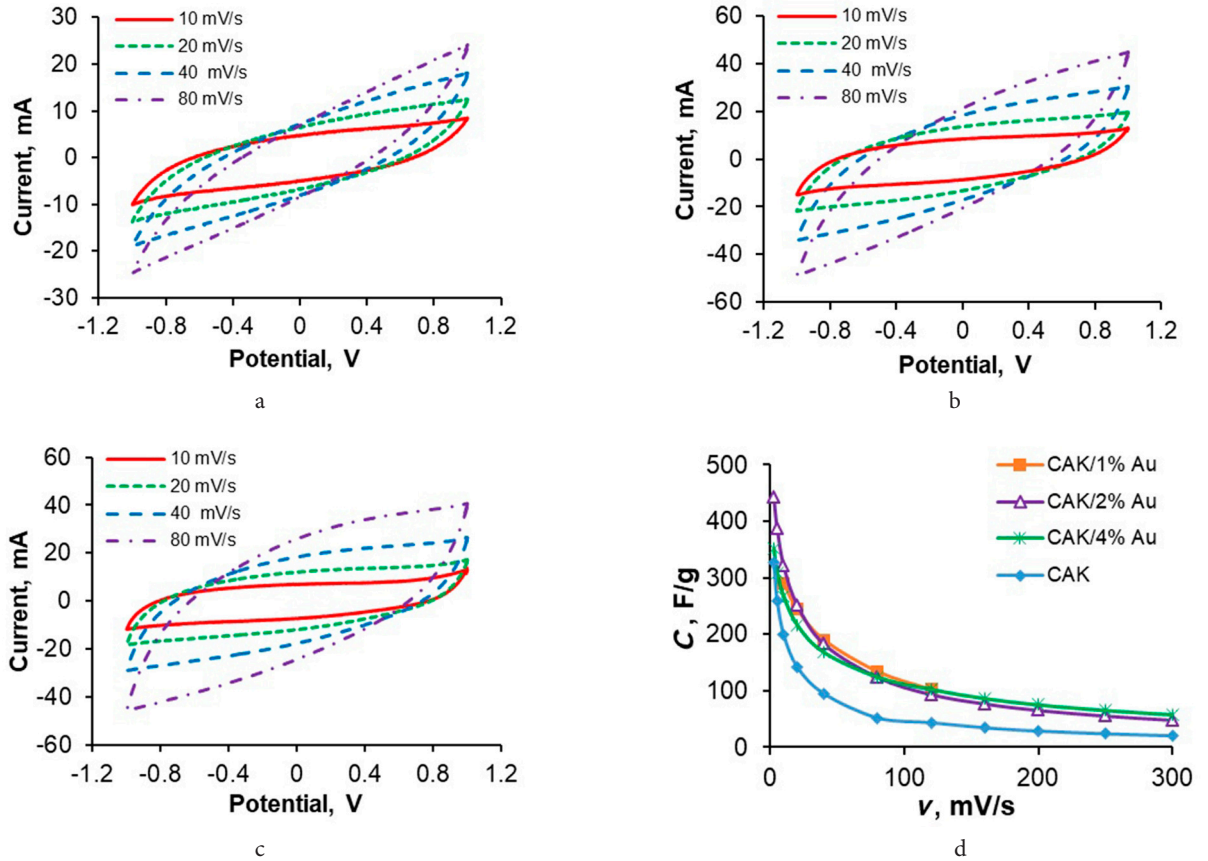

Fig. 5. (Color online) CV curves of a symmetrical cell with electrodes based on CAK matrix (a) and asymmetric cells with working electrodes based on NSC CAK/2% Au (b) and CAK/4% Mn_xO_y (c). Dependences of the electrode specific capacitance on the potential scan rate (d).

The observed dependence of the specific electrical capacitance on the scanning rate is associated with the diffusion limitation of the charge accumulation in EDL at the "micropore surface/electrolyte" interface; therefore, the effect of an increase in capacitance with a decrease in the scanning rate is noticeably stronger for microporous CAK HPCM. A decrease in the potential scan rate partially removes diffusion limitation, and ever smaller micropores begin to participate in the charge accumulation.

An increase in the electric capacitance at the high scanning rates in the presence of the Au filler is associated with a more active charge accumulation in EDL at the "external surface of the HPCM/Au aggregates/electrolyte" interface. The effect for Boghead/Au is more noticeable, since Au NPs deposited on the surface of mesopores are involved in the process. The observed effect of Mn_xO_y over the entire range of scanning rates indicates relatively high rates of Red-Ox reactions involving Mn_xO_y NPs, which was previously noted for NSC MWCNT/Mn_xO_y [19].

A sharper increase in capacitance for NSCs based on the Boghead matrix with a decrease in scanning speed compared to NSCs based on CAK (Figs. 4 d and 5 d) can be associated with partial decoration of micropores in the Boghead HPCM by nanoparticles (Table 2), while for NSC based on CAK, due to the weaker effect of fillers on micropores, the absolute effect of their introduction practically does not depend on the scanning speed (Fig. 5 d).

4. Conclusions

Due to the complex surface texture of the considered C-matrices and the high tendency of NP fillers to aggregation, it is not possible to achieve NSC surface decoration (including meso- and micropores) with nano-thick filler quasi-films. It has been shown that fillers are deposited in the form of aggregates on the outer C-matrice surfaces, and only in Boghead based NSCs they are formed on the meso- and micropore surfaces in relatively small amounts. The maximum effects of increasing the electrical capacitance relative to the matrix capacitance achieved (in the region of high scanning rates) were for NSC: SWCNT/2%Au by a factor of 4.5, SWCNT/2%Mn_xO_y (4.5-fold), Boghead/1%Au (1.9-fold), Boghead/4%Mn_xO_y (2.6-fold), CAK/2%Au (2.9-fold) respectively; in the region of low scanning rates: NSC SWCNT/2%Au by a factor 2.8, SWCNT/2%Mn_xO_y (2.6-fold), Boghead/1%Au (1.3-fold), Boghead/4%Mn_xO_y (1.3-fold), CAK/2%Au (1.4-fold), respectively.

For HPCM, Mn_xO_y is a more effective filler, which causes an increase in the specific capacitance due to the pseudocapacitance addition as a result of electrode redox reactions. For SWCNT-based NSCs, filling with Au NPs is most efficient.

The realization of such significant relative effects with the achievement of sufficiently high values of the specific electrical capacitance of NSCs (up to 450 – 650 F/g) makes it possible to consider the composites as promising materials for the development of SC electrodes. In this regard, further efforts to improve their functional characteristics are expedient, for example, finding the conditions for decorating the surface with nanolayers of fillers without blocking the pores of the matrices, with an increase in the degree of surface coverage.

Acknowledgments. The work was carried out within the framework of the projects of the Ministry of Education and Science (EGISU No. 121031500211-9) and RFBR 20-43-420017/20, using the equipment of the Centre for Collective Use of the FRC CCC SB RAS. The authors are grateful for the TUBALL samples provided by OCSiAl (Novosibirsk), Ph. D. Sozinov S. A. and Ph. D. Russakov D. M. (CCU of FRC CCC SB RAS, Kemerovo) for studying the samples by scanning (SEM) and transmission (TEM) electron microscopy.

References

1. Z. Zhai, L. Zhang, T. Du, B. Ren, Y. Xu, S. Wang, J. Miao, Z. Liu. Mater. Des. 221, 111017 (2022). Crossref
2. R. Kumar, E. Joanni, S. Sahoo, J.-J. Shim, W. K. Tan, A. Matsuda, R. K. Singh. Carbon. 193, 298 (2022). Crossref
3. P. Xie, W. Yuan, X. Liu, Y. Peng, Y. Yin, Y. Li, Z. Wu. Energy Storage Mater. 36, 56 (2021). Crossref
4. R. Wang, X. Li, Z. Nie, Y. Zhao, H. Wang. J. Energy Storage. 38, 102479 (2021). Crossref
5. S. Kour, S. Tanwar, A. L. Sharma. Mater. Today Commun. 32, 104033 (2022). Crossref
6. G. Y. Simenyuk, Y. A. Zakharov, N. V. Pavelko, V. G. Dodonov, V. M. Pugachev, A. V. Puzynin, T. S. Manina, C. N. Barnakov, Z. R. Ismagilov. Catal. Today. 249, 220 (2015). Crossref
7. N. Afsarimanesh, A. Nag, Md. Eshrat e Alahi, S. Sarkar, S. Mukhopadhyay, G. S. Sabet, M. E. Altinsoy. Sens. Actuator A: Phys. 344, 113743 (2022). Crossref
8. E. Dhandapani, S. Thangarasu, S. Ramesh, K. Ramesh, R. Vasudevan, N. Duraisamy. J. Energy Storage. 52 (C), 104937 (2022). Crossref
9. Y. Zakharov, G. Simenyuk, V. Pugachev, V. Dodonov, T. Trosnyanskaya, Z. Ismagilov, E. Kachina, D. Yakubik. Energy Technol. 9 (11), 2100449 (2021). Crossref
10. Y. Fang, Q. Zhang, L. Cui. Microporous Mesoporous Mater. 314, 110870 (2021). Crossref
11. M. R. Predtechenskiy, A. A. Khasin, A. E. Bezrodny, O. F. Bobrenok, D. Y. Dubov, V. E. Muradyan, V. O. Saik, S. N. Smirnov. Carbon Trends. 8, 100175 (2022). Crossref
12. N. I. Fedorova, I. Y. Zykov, Z. R. Ismagilov. Coke Chem. 65 (5), 201 (2022). Crossref
13. G. Y. Simenyuk, Y. A. Zakharov, A. V. Puzynin, C. N. Barnakov, T. S. Manina, Z. R. Ismagilov, A. A. Vladimirov, N. V. Ivanova, V. M. Pugachev, V. G. Dodonov. Mater. Manufact. Proc. 31 (6), 739 (2016). Crossref
14. G. Y. Simenyuk, Y. A. Zakharov, V. M. Pugachev, V. G. Dodonov, T. O. Trosnyanskaya, T. S. Nechaeva, L. V. Ilkevich, E. S. Mikhailova, Z. R. Ismagilov. Chem. Sustain. Develop. 26 (6), 609 (2018).
15. T. A. Larichev, Yu. A. Zakharov, N. M. Fedorova, G. Yu. Simenyuk, V. M. Pugachev, V. G. Dodonov, D. G. Yakubik, T. O. Trosnyanskaya. Chem. Sustain. Develop. 29 (5), 552 (2021). Crossref
16. T. A. Larichev, N. M. Fedorova, Y. A. Zakharov, G. Y. Simenyuk, V. M. Pugachev, V. G. Dodonov, E. V. Kachina,

E. S. Mikhailova. Chem. Sustain. Develop. 26 (6), 619 (2018).
17. S. A. Semenova, T. S. Manina, N. I. Fedorova, Z. R. Ismagilov, T. I. Gulyaeva, N. N. Leont'eva, V. A. Drozdov. Solid Fuel Chem. 47 (5), 292 (2013). Crossref
18. Y. A. Zakharov, G. Y. Simenyuk, T. S. Manina, C. N. Barnakov, V. M. Pugachev, V. G. Dodonov, N. V. Pavelko. Nanotechnol. Russ. 10 (5-6), 388 (2015). Crossref
19. Y. A. Zakharov, G. Y. Simenyuk, E. V. Kachina, Y. N. Dudnikova, V. G. Dodonov, Z. R. Ismagilov. Inorg. Mater. 57 (5), 487 (2021). Crossref
20. B. Ullah, Y. Cheng, L. Wang, W. Yang, I. M. Jiskani, B. Hu. Int. J. Coal Sci. Technol. 9 (1), 58 (2022). Crossref
21. R. Bardestani, G. S. Patience, S. Kaliaguine. Can. J. Chem. Eng. 97, 2781 (2019). Crossref
22. L. Leng, Q. Xiong, L. Yang, H. Li, Y. Zhou, W. Zhang, S. Jiang, H. Li, H. Huang. Sci. Total Environ. 763, 144204 (2021). Crossref
23. M. Thommes, K. Kaneko, A. V. Neimark, J. P. Olivier, F. Rodriguez-Reinoso, J. Rouquerol, K. S. W. Sing. Pure Appl. Chem. 87 (9–10), 1051 (2015). Crossref
24. Y. A. Zakharov, G. Y. Simenyuk, T. O. Trosnyanskaya, V. M. Pugachev, D. M. Russakov, T. A. Larichev. Chem. Sustain. Develop. 30 (5), 507 (2022). (in Russian) Crossref
25. C. Y. Foo, H. N. Lim, M. A. Mahdi, M. H. Wahid, N. M. Huang. Sci. Rep. 8, 7399 (2018). Crossref
26. K. N. Chaudhari, S. Chaudhari, J.-S. Yub. J. Electroanal. Chem. 761, 98 (2016). Crossref
27. P. M. Anjana, M. R. Bindhu, R. B. Rakhi. Mater. Sci. Energy Technol. 2 (3), 389 (2019). Crossref
28. R. R. Kannan, N. Lenin, A. A. Banu, M. Sivabharathy. Mater. Lett. 314, 131887 (2022). Crossref
29. B. S. Singu, E. S. Goda, K. R. Yoon. J. Ind. Eng. Chem. 97, 239 (2021). Crossref